

Changes in the measured image separation of the gravitational lens system, PKS 1830-211.

C. Jin,¹ M.A. Garrett,² S. Nair,³ R.W. Porcas,⁴ A.R. Patnaik,⁴ R. Nan¹

¹*National Astronomical Observatories, Chinese Academy of Sciences, A20 Datun Road, Chaoyang District, Beijing 100012, China*

²*Joint Institute for VLBI in Europe, Postbus 2, 7990 AA Dwingeloo, The Netherlands*

³*Raman Research Institute, C.V. Raman Avenue, Bangalore 560080, India*

⁴*Max-Planck-Institut für Radioastronomie, Auf dem Hügel 69, D-53121 Bonn, Germany*

Accepted 2003 January 8. Received 2002 March 13; in original form 2002 March 7

ABSTRACT

We present eight epochs of 43 GHz, dual-polarisation VLBA observations of the gravitational lens system PKS 1830-211, made over fourteen weeks. A bright, compact “core” and a faint extended “jet” are clearly seen in maps of both lensed images at all eight epochs. The relative separation of the radio centroid of the cores (as measured on the sky) changes by up to 87 μ as between subsequent epochs. A comparison with the previous 43 GHz VLBA observations (Garrett et al., 1997) made 8 months earlier show even larger deviations in the separation of up to 201 μ as. The measured changes are most likely produced by changes in the brightness distribution of the background source, enhanced by the magnification of the lens. A relative magnification matrix that is applicable on the milliarcsecond scale has been determined by relating two vectors (the “core-jet” separations and the offsets of the polarised and total intensity emission) in the two lensed images. The determinant of this matrix, $-1.13 (\pm 0.61)$, is in good agreement with the measured flux density ratio of the two images. The matrix predicts that the 10 mas long jet, that is clearly seen in previous 15 and 8.4 GHz VLBA observations (Garrett et al. 1997, Guirado et al. 1999), should correspond to a 4 mas long jet trailing to the south-east of the SW image. The clear non-detection of this trailing jet is a strong evidence for sub-structure in the lens and may require more realistic lens models to be invoked *e.g.* Nair & Garrett (2000).

Key words: methods: data analysis: techniques: image processing: cosmology: gravitational lensing: individual (PKS 1830-211)

1 INTRODUCTION

PKS 1830-211 is a very bright and highly variable radio source at cm- and mm-wavelengths (Romero et al., 1997). As well as being a double-imaged gravitational lens system (Rao & Subrahmanyan 1988, Jauncey et al. 1991), it is also identified by the EGRET instrument on the Compton Gamma-ray Observatory as an unusually strong source of gamma-rays (Mattox et al., 1997). The radio and gamma-ray properties suggest that the background source in this system is best classified as a blazar (Jin et al., 1999). The source lies close to the galactic plane, and optical identifications and redshift determinations have been severely handicapped by the high level of dust obscuration along the line-of-sight. However, optical and infrared observations at Keck and ESO (Courbin et al. 1998, Frye et al. 1999) and infrared observation using HST (Lehár et al., 2000) have identified both of the flat spectrum radio cores. Recently, the ESO

New Technology Telescope(NTT) near infra-red spectra show clear detections of both the H_{α} and H_{β} emission lines, implying a source redshift of $z_s = 2.507$ (Lidman et al., 1999). The lens may be a compound system: molecular absorption at $z = 0.886$ (Wiklind & Combes, 1996) and HI absorption at $z = 0.19$ (Lovell et al., 1996) have been detected. A time delay (26^{+4}_{-5} days (Lovell et al., 1998); 24^{+5}_{-4} days (Wiklind & Combes, 1999)), and a magnification ratio of 1.52 ± 0.005 (Lovell et al., 1998) have been measured for the two compact core images in the system.

Previous high resolution radio observations of the source show two lensed images, with a separation of about 1 arcsec (Rao & Subrahmanyan, 1988). MERLIN and VLA observations revealed an elliptical Einstein ring connecting the two brighter components (Jauncey et al., 1991). Subsequent VLBI observations (Garrett et al. 1997, Guirado et al. 1999) have revealed detailed structures in both of the two lensed images. VLBI observations at 8.4 GHz

(Guirado et al., 1999), 15 GHz (Garrett et al., 1997) and 22 GHz (Jones et al., 1996), show significant differences between the north-eastern (NE) and south-western (SW) images on the milliarcsecond (mas) scale. In particular, a prominent 10-mas-long jet associated with the core of the NE image, has no obvious counterpart in the SW image. Nair & Garrett (2000) attempt to explain this results as due to a perturbation in the NE image by a lens of globular cluster scale. The first 43 GHz maps also showed relatively rapid changes in the brightness distribution of the images (Garrett et al., 1997), an effect that may be partly explained by the magnification provided by the lens system. According to models of this system, the magnification between the images and background source, may be as large as 5 - 10 (Kochanek & Narayan 1992, Nair et al. 1993).

In this paper, we present 8-epoch, VLBA 43 GHz maps of both lensed radio images, in both polarised and total intensity. In the following section, a brief summary of the observations and data analysis are presented. Measured changes in separation between the radio core images are presented and discussed in section 3, together with the determination of a magnification matrix that relates the two images on the milliarcsecond scale. A summary of the main results is presented in section 4.

2 OBSERVATION AND DATA REDUCTION

PKS 1830-211 was observed using the VLBA at 43 GHz at eight separate epochs, over a period of 14 weeks (1997 January 19 - 1997 April 30). The source was observed for a total of 5 hours at each epoch. And each epoch was separated in time by about 14 days. For all observations right and left hands of polarisation were recorded in 2-bit mode, each with a total bandwidth of 32 MHz, divided into 4 IF channels. Several nearby and compact calibrators (B 1730-130, B 1749+096, B 1741-038, and B 1908-211) were observed every 18 minutes - at the beginning and end of each 22 minute tape pass. Both parallel and cross-hand polarisation products were generated by the NRAO VLBA correlator in Socorro, NM, USA. Only one processing centre was employed, positioned mid-way between the NE and SW images. In order to avoid the effects of time smearing, very short integrations times were provided by the correlator (0.39 s).

The data quality was generally good except for the sixth epoch (1997 April 3) which was adversely affected by bad weather at Kitt Peak, excessive noise and resulting weak fringes at Brewster and bad playback at Fort Davis (for some but not all IF channels). Nevertheless, the data for the sixth epoch were still reasonable after appropriate editing of the data. Initial calibration of the data was performed with the AIPS package. The visibility amplitudes were calibrated using the system temperatures and gain information provided by each telescope. Residual delays and fringe rates associated with instrumental effects were determined from the calibrators and removed from the target source data (PKS 1830-211). Hybrid mapping of the calibrators also generated antenna based amplitude gain corrections and these were also applied and interpolated to PKS 1830-211. The instrumental polarisation calibration was derived from the compact calibrators (following

Leppänen et al., 1995) and applied to PKS 1830-211. The polarization angle was not calibrated, since we were more interested in a comparison of the polarization intensity and angle between the two lensed images which didn't require any absolute angle to be determined. At all eight epochs, the D-terms (so-called *leakage factors*) solved are about 4-8 % for BR, HN and LA and less than 5 % for the other seven antennas in the VLBA array.

Large residual rates associated with atmospheric instabilities remained in the target data and this necessitated fringe-fitting PKS 1830-211 directly. Due to the complicated nature of the source, it was first necessary to produce an initial model of the source (containing both images) using the (calibrator) corrected data. Preliminary total intensity HYBRID maps of both lensed images were made using wide-field techniques (Garrett et al., 1999), and these were later used as a model for fringe-fitting. After this final round of fringe-fitting the corrections were applied to PKS 1830-211.

In order to reduce the size of the calibrated data set, each of the individual IFs were averaged in frequency - the final data set being composed of 4 independent (but contiguous) 8 MHz channels (for each parallel and cross hand polarisation product). The calibrated data were also averaged in time in a baseline dependent manner (integration times ranged from 0.39 to 15 seconds depending on the projected baseline length). Hybrid maps of both lensed images were made simultaneously from this data set.

The naturally weighted contour maps of total and polarised intensity are shown in Fig. 1 and Fig. 2. The FWHM of the circular restoring beam is 0.5 mas. The off-source rms noise level is about 0.8 mJy beam⁻¹ in total intensity, and 0.3 mJy beam⁻¹ in polarised intensity maps at all eight epochs. A bright, compact "core" and a fainter more extended "jet" are clearly seen on both of the NE & SW images at all epochs. Each of these core and jet components was fitted by a single elliptical Gaussian component using AIPS task IMFIT except for the much weaker "jet" on the NE image at the 6th epoch, where the low flux density prevents reasonable model-fitting. One elliptical Gaussian component was used to fit the single component observed in the polarised maps of both the NE & SW images. The results are presented in Table 1.

3 RESULTS AND DISCUSSION

3.1 The angular separation between the NE and SW images

After fitting Gaussians to the NE and SW core components, we measured the angular separation between the centroids of the core radio emission. We take this as an indicator of the separation between the two images, since the core is well defined across all epochs. And the core is much brighter, thus the errors on the positions are much smaller. The uncertainty of the positions of the fitted Gaussian components are estimated by the following formula:

$$\Delta X \sim \frac{\Theta(\text{beam})}{2} \cdot \frac{1}{\text{SNR}} \cdot \sqrt{1 + \left(\frac{\Theta(\text{imagesize})}{\Theta(\text{beam})}\right)^2}$$

where SNR is the signal-to-noise ratio of the component, which is determined by dividing the peak flux density of the

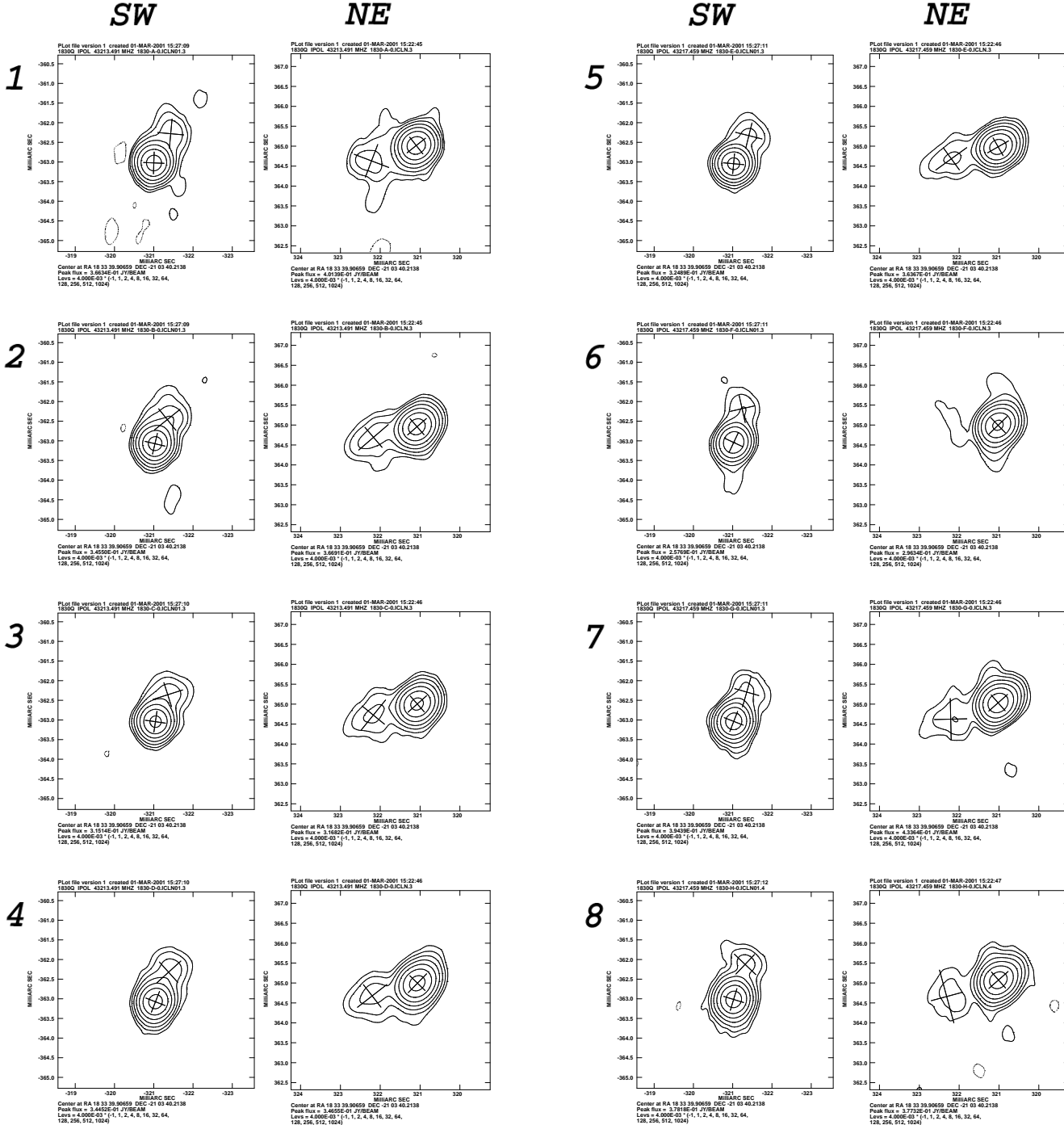


Figure 1. Total intensity contour maps of the SW and NE images for all eight epochs. The epoch of observation increases from top to bottom, left to right. Contours are spaced by factors of two in brightness, with the lowest at five times the r.m.s. noise of 0.8 mJy per beam. All maps are on the same scale. The FWHM of the circular restoring beam is 0.5 mas. The crosses superimposed on the maps represent the position and extent of the fitted Gaussian components. The measured time-delay of 26_{-5}^{+4} days implies that structure in the NE image at one epoch corresponds to that in the SW image roughly two epochs later.

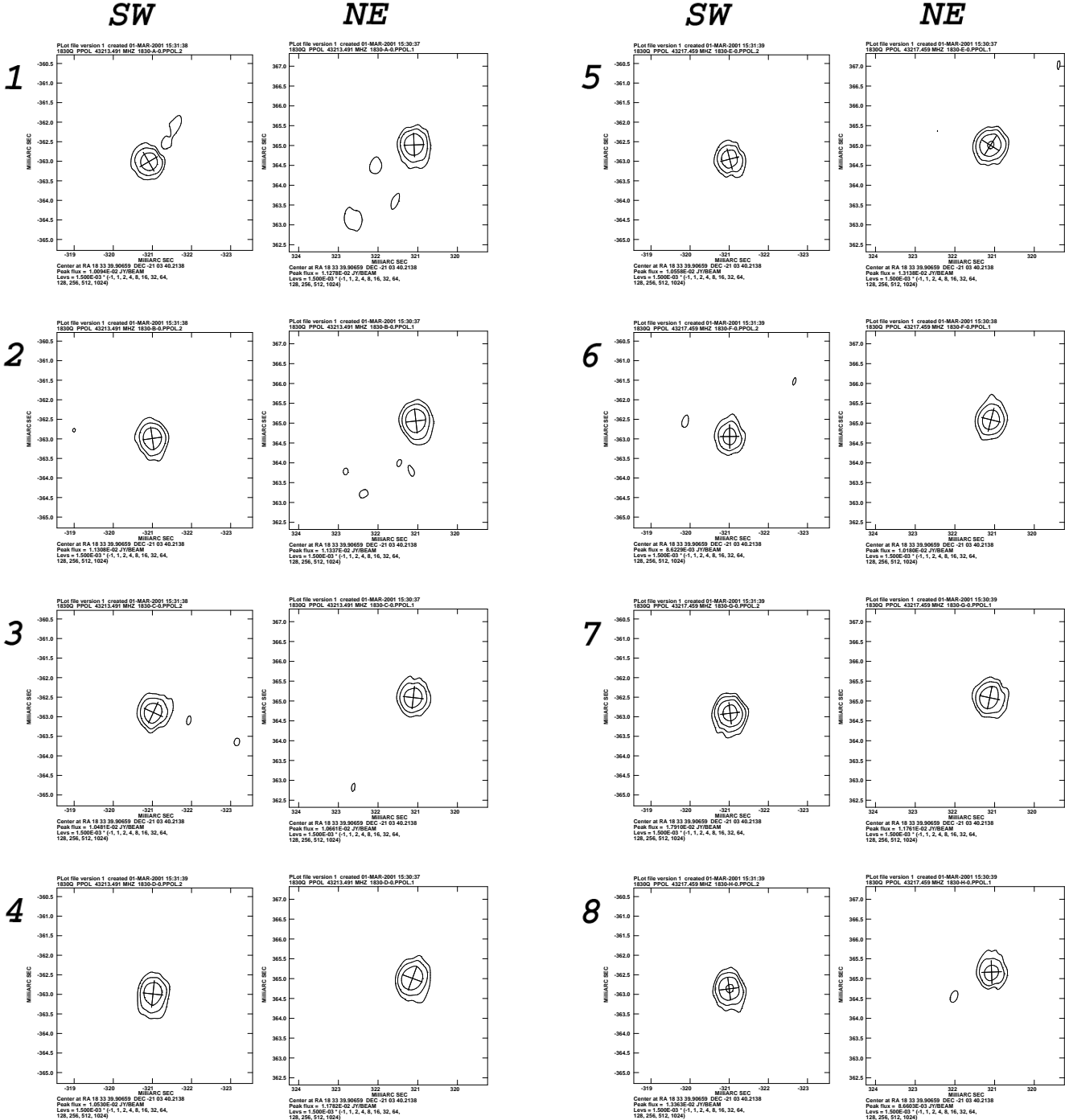


Figure 2. Polarised intensity contour maps of the SW and NE images for all eight epochs. The epoch of observation increases from top to bottom, left to right. Contours are spaced by factors of two in brightness, with the lowest at five times the r.m.s. noise of 0.3 mJy per beam. All maps are on the same scale. The FWHM of the circular restoring beam is 0.5 mas. The crosses superimposed on the maps represent the position and extent of the fitted Gaussian components. The measured time-delay of 26_{-5}^{+4} days implies that structure in the NE image at one epoch corresponds to that in the SW image roughly two epochs later.

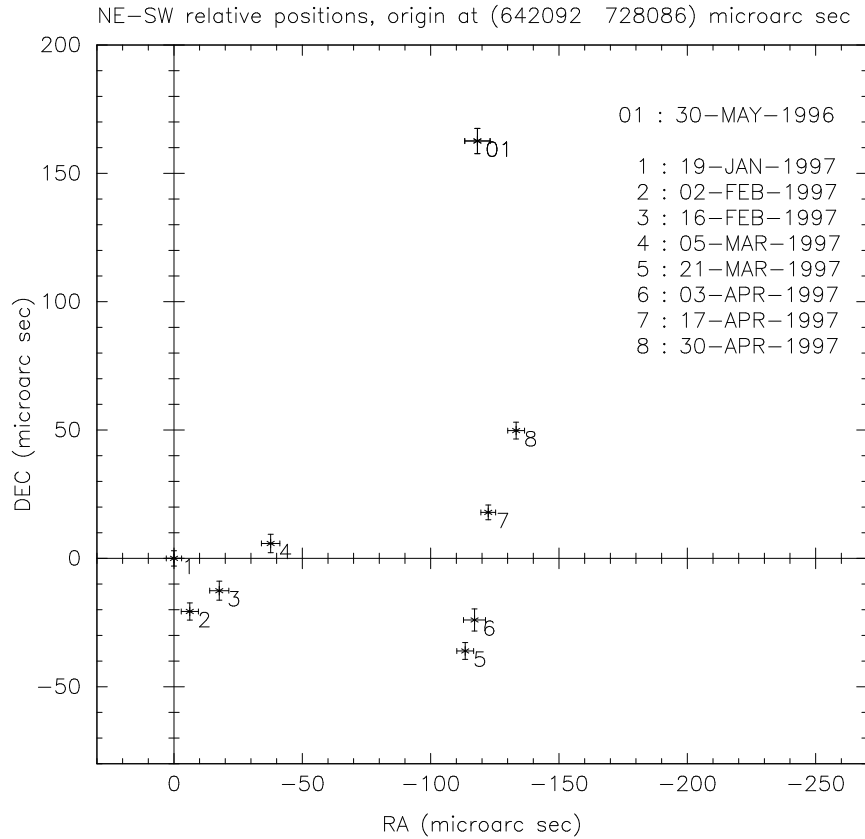


Figure 3. Deviations in the angular separation of the NE and SW core images. The nominal origin of these deviations is defined to be $+642071.312\mu\text{as}$ and $+727990.0\mu\text{as}$. The numbers associated with each of the deviations (see crossed symbols) indicates the epoch of the observation.

Table 1. Total flux densities (in mJy) of the Gaussian fitted components on the images. From left to right, we present the total flux intensiy of the core, jet and polarised core for the NE and SW images.

epoch	NE I-core	NE I-jet	NE P-core	SW I-core	SW I-jet	SW P-core
1997 Jan 19	505.7 ± 2.4	72.6 ± 3.7	13.2 ± 0.4	428.2 ± 2.2	57.4 ± 3.0	11.2 ± 0.3
1997 Feb 02	485.1 ± 2.5	64.2 ± 3.9	14.3 ± 0.4	386.1 ± 2.2	73.4 ± 3.4	12.9 ± 0.3
1997 Feb 16	415.3 ± 2.5	54.7 ± 3.9	11.9 ± 0.3	353.3 ± 2.2	53.6 ± 3.2	12.3 ± 0.4
1997 Mar 05	478.1 ± 2.6	59.9 ± 3.7	15.2 ± 0.4	406.0 ± 2.2	62.3 ± 3.4	14.1 ± 0.4
1997 Mar 21	449.8 ± 2.4	49.2 ± 3.8	14.2 ± 0.3	348.6 ± 2.1	36.7 ± 2.8	10.5 ± 0.3
1997 Apr 03	385.9 ± 2.5	$-- \pm 2.0$	11.6 ± 0.3	291.9 ± 2.2	30.2 ± 2.9	9.8 ± 0.3
1997 Apr 17	569.0 ± 2.5	53.4 ± 4.1	13.6 ± 0.3	447.3 ± 2.2	42.9 ± 3.1	19.3 ± 0.3
1997 Apr 30	511.5 ± 2.6	51.6 ± 5.5	9.7 ± 0.3	459.9 ± 2.3	44.3 ± 3.0	14.5 ± 0.3

fitted Gaussian component by the post-fit r.m.s. error ^{*} associated with the pixels in the image. Notice that the aberration effect, which is mainly caused by the earth's orbital motion around the sun, will cause an apparent position shift of a source. The amount of the shift(aberration) is a function of the position of the source and the time of a year when the source is observed. Considering two fixed sources on the sky, this will make the measured apparent separation between the two sources different from the real separation. And further, the difference will change at different time of a year. In our case, for the NE & SW

^{*} The post-fit r.m.s. error is derived from the difference between the Gaussian model and the data, for the pixels in the lensed image.

images of the gravitational lens system, this instantaneous differential aberration changes by up to several tens μas across the epochs, much larger than the positional accuracy of our measurements. In order to compare the separations across the epochs, we have to take these effects into account. We subtracted the aberrations of the NE & SW images from the apparent separation at each epoch. Thus got the real separations between the two lensed images at each epoch. The final results are presented in Fig. 3. In the figure, we defined a nominal separation between the core images to be that measured at the first epoch of observations, viz., $+642092\mu\text{as}$ (RA) and $+728086\mu\text{as}$ (Dec), relative to the SW core. We plot deviations from this nominal separation (also relative to the SW core) for each epoch. We have also included the previous observation (01:30-MAY-1996) in this

figure. It can be clearly seen that the relative separation between the images of the core changes with epoch. The largest overall deviation of up to 142 μ as occurs at the 8th epoch (1997 April 30). The largest deviation measured between successive epochs is 87 μ as (epochs 4 and 5).

A comparison of the nominal separation of the NE and SW core images with previous 43 GHz VLBA observation (Garrett et al., 1997) made 8 months earlier show even larger deviations of 201 μ as.

We have considered several possible *extrinsic* explanations for this observed change in the angular separation of the images. These include: induced shifts in the centroids of the core brightness distribution due to milli-lensing by massive ($10^3 - 10^4 M_\odot$) compact objects in the halo of the lens (Wambsganss & Paczynski, 1992); and the relative proper motion between the NE and SW images caused by the transverse velocity of the lens galaxy across the sky (Kochanek et al., 1996), though the image separation does not necessarily change with changing source position. However, neither of these effects can reproduce the magnitude of the measured deviations on either the shortest (a few weeks) or longest time scales (11 months) considered here. In addition, the effect of “image wander”—an apparent shift in the position of a source caused by Galactic scattering (Rickett, 1990), also seems to be an unlikely explanation for the changing image separations at this frequency. In particular, the SW deconvolved core size of $\sim 0.6 \times 0.2$ mas at 1.3 cm (Jones et al., 1996) and our measurement of $\sim 0.228 \times 0.148$ mas at 7 mm scales almost linearly with λ as expected from simple models of synchrotron radio emission. A λ^2 law would be expected in the case of ISS (indeed this is observed at longer cm wavelengths (Jones et al., 1996)). This suggests that the measured source size is dominated by its internal radio structure, and that any interstellar scattering effects are rather weak at λ 7 mm.

We believe that the most likely explanation for the changing image separation involves continuous changes in the brightness distribution of the background radio source on relatively short-time scales (considerably shorter than that usually probed by VLBI). As the centroid of the radio emission of the background radio source moves within the source plane, the separation of the images changes. In addition, the position of one image lags behind the other (the motions being separated by the time-delay). The changes in the measured angular separation are a combination of both effects.

For a FRW universe ($\Omega_o = 0.3$, $\lambda_o = 0.7$, $H_0 = 70 \text{ km s}^{-1} \text{ Mpc}^{-1}$), the shift of $\approx 80 \mu$ as (the largest shift between successive epochs separated by 16 days) corresponds to a linear distance of ≈ 0.45 pc at $z_s = 2.507$. Even if one takes into account the magnification provided by the lens (a factor of ~ 10 according to (Kochanek & Narayan, 1992)(Nair et al., 1993)), a shift of 80 μ s scales to ≈ 0.14 pc, thus implying (unlensed) superluminal velocities in the rest frame of the background source in excess of 10 c . Given the blazar nature of the background source, and the apparently chaotic structure surrounding the cores at 43 GHz (Garrett et al., 1997) which implies the radio jet in 1830-211 is well beamed towards us, the measured superluminal velocity of 10 c might be expected. Another EGRET source 1156+295 (Mattox et al., 1997),

NE/SW total flux density ratios

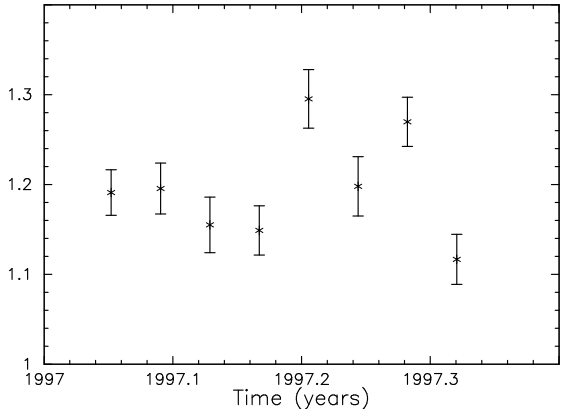


Figure 4. The flux density ratio between NE and SW image as a function of time.

which is probably similar to the background source of 1830, also showed superluminal velocity of several c (Glenn Piner et al., 1997), but across 10 epochs spanning a period of 8 years. The detection of source evolution in 1830 on these short time-scale of several weeks would be impossible if it were not for the fact that this is a lensed system which provides us with a magnified view and closely spaced multiple images that allow accurate relative position measurements to be made.

3.2 The relative magnification matrix

3.2.1 Determination of the relative magnification matrix

Based on flux density ratio arguments, we can directly relate the “core” and the “jet” in one image to that in the other image. In addition, we also note that both images are also weakly polarised, with the position of the polarised emission being significantly offset from the position of the total intensity core emission. We therefore identify two vectors in each lensed image: the vector defined by the core-jet structure and the vector defined by the positional offset of the polarised emission from the total intensity core position. These vectors were used to determine a magnification matrix, M_{SW2NE} , that relates the brightness distribution of the SW image to that observed in the NE image.

Figure 5 shows the vectors corresponding to the positions of the “jet” and the polarised peak with respect to the “core”. Both of the vectors vary through the 8 epochs of observation but the changes are not obviously systematic (e.g. there is no clear, linear proper motion of the secondary component with respect to the core). We have determined the error-weighted averages for these quantities over all epochs of observation. Since there is a measured time-delay of 26^{+4}_{-5} (Lovell et al., 1998) days, we have exclude the first two epochs of the SW image and the last two epochs of the NE image in the averaging process. The uncertainty of each averaged vector is estimated from the scattering of the vector through the epochs.

Using these data we estimate M_{SW2NE} :

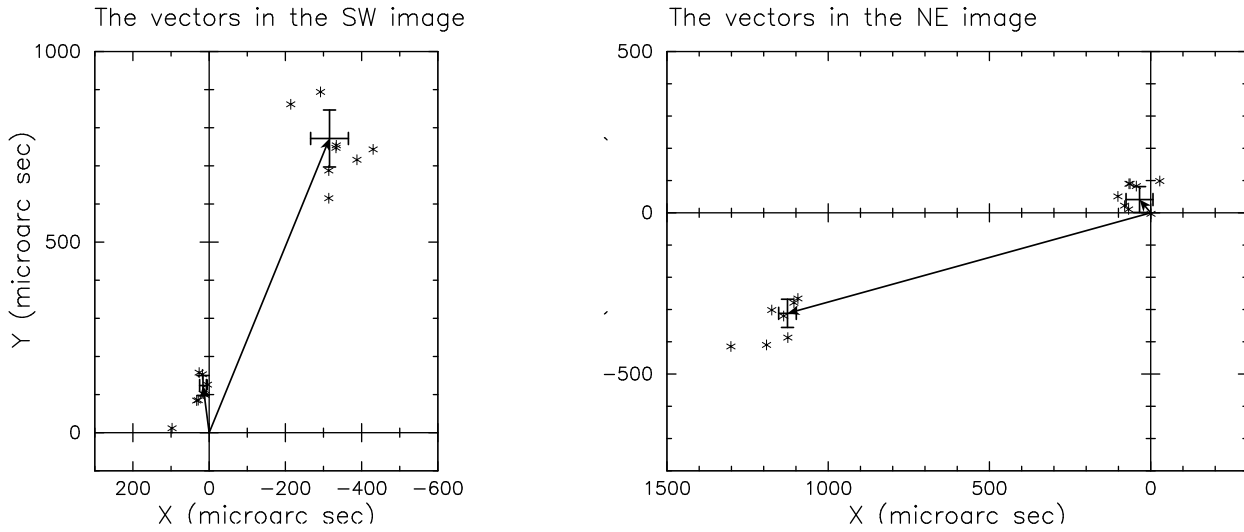


Figure 5. The two set of vectors in the NE(right) and SW(left) images. The core-jet separations have larger amplitudes compared with the offsets between the centroids of the polarised and total intensity emission.

$$M_{(SW2NE)} = \begin{vmatrix} -2.20 \pm 0.50 & 0.56 \pm 0.19 \\ 1.38 \pm 0.43 & 0.16 \pm 0.17 \end{vmatrix}.$$

The errors (1σ) are estimated from Monte Carlo simulations. The determinant of the matrix is: -1.13 ± 0.61 (1σ). The sign of the determinant indicates the two images have opposite parities as predicted by lens models of the system. The magnitude of determinant is consistent with Lovell et al.'s (1998) measurement for the flux density ratio (NE:SW) of 1.52 ± 0.005 , and our own measurements through the 8 epochs of observation, presented in Fig 4. The ratio (NE:SW) changes with epoch, ranging from 1.1 to 1.4, in good agreement with the determinant of the matrix (determined purely from positional information only). The changes of the ratio are most likely due to intrinsic brightness changes in the background radio source combined with the time-delay between the images (changes in the SW image lag behind the NE image by 3-4 weeks).

3.2.2 Applying the matrix to previous VLBI observations

We have applied our matrix to previous VLBA 15 GHz observations of PKS 1830-211 (Garrett et al., 1997). We find that the peak of the faint extended component that lies approximately (-5.0, 5.0)mas to the north-west of the 15 GHz SW core, maps to (13.8, -6.1)mas to the south-east of the NE core in the NE image with an uncertainty of 2.2 mas(1σ). This overlaps with the extended component that lies approximately 13 mas to the south-east of the 15 GHz NE core. Given that the positions of these faint components are not very well defined (due to their extended nature), this close correspondence strongly suggests that these features are associated, multiply-lensed emission.

Our new matrix *cannot*, however, explain the fact that the prominent 10-mas-long jet, clearly seen emerging from the core of the NE image at 15 GHz in a north-westerly direction, has no obvious counterpart in the SW image. The

matrix predicts that the position of the hot-spot at the tip of the jet, approximately 10 mas to the north-west of the NE core, should map on to a region located 5 mas to the south-east of the SW core with an uncertainty of tens of mas(1σ). This large positional uncertainty makes it difficult to identify the jet's counterpart in the SW image. Even if we ignore this large uncertainty, such emission, including the rest of the extended jet, should have been easily detectable at 15 GHz and 8.4 GHz. Nair & Garrett (2000) have recently attempted to explain the apparently singular jet in the NE image as a perturbation in the lens potential probed by that image. In their model Nair and Garrett argue that this perturbation arises from sub-structure in the lens e.g. the chance alignment of the NE radio image with a massive discrete structure, such as a globular cluster in the lens galaxy.

3.3 The flux ratios

Since the VLBA observations at 43 GHz were severely affected by the atmospheric opacity effect, so the absolute flux density scale in Table 1 varied between one epoch and another. Thus it is not possible to get meaningful light curves from the fluxes presented in Table 1. However, taking the data from Table 1, we have considered various flux density ratios in the two images. The core-jet flux density ratio and the fractional polarisation of the two images change with epoch, but neither of these two ratios show obvious correlation after the time-delay of 24^{+5}_{-4} days has been compensated for. The jet components in the two images are normally more extended, thus making their flux density estimates less accurate than that of the core components. If the source has detailed polarisation structure that can not be resolved by the VLBI array, the polarisation flux density measurement will also have large errors. In the light of the above, the results obtained are not surprising.

4 SUMMARY

We have presented eight-epoch, 43 GHz, dual-polarisation VLBA observations of the gravitational lens system, PKS 1830-211. “Core-jet” structure was clearly seen in both lensed images at all epochs. The position of the polarised intensity emission is observed to be offset from the peak of total intensity maps. The offset is about one third of the synthesised beam and is observed at all eight epochs and in both images.

The relative separation between the “core” centroid positions of the two lensed images changes by up to $87 \mu\text{as}$ between subsequent epochs. A comparison of these recent separation measurements with previous 43 GHz observations (Garrett et al., 1997) shows even larger deviations of up to $201 \mu\text{as}$ over a period of 27 weeks. The measured changes are most likely produced by evolution in the brightness distribution of the background source, enhanced by the magnification of the lens.

The multi-component core-jet radio structure observed in both images, together with the spatial offset between the polarised and total intensity core emission, permit us to estimate a relative magnification matrix for this system. The determinant of the matrix is -1.13 ± 0.61 , in good agreement with the flux density ratio of the images. The matrix presented here can be an important input for the construction of realistic lens models for this system and thus associated estimates of H_0 .

Application of this matrix to previous VLBI observations meets with mixed success. In one case it is reasonably successful in relating a faint extended component observed in each of the NE and SW images at 15 GHz. However, it also predicts that the extremely prominent 10-mas-long jet associated with the 15 GHz NE image, should be easily detected in the SW image. The fact that the high quality 15 GHz and 8.4 GHz VLBA observations (Garrett et al. 1997, Guirado et al. 1999) do not detect such a jet, provides strong evidence for sub-structure in the lens. More realistic, multi-component lens mass distributions probably need to be invoked (*e.g.* Nair & Garrett (2000)).

ACKNOWLEDGMENTS

This research was supported by the grant for collaborative research in radio astronomy of the Royal Dutch and Chinese Academies of Science (KNAW and CAS) and was also partially supported by a grant from the NSFC. The National Radio Astronomy Observatory is a facility of the National Science Foundation operated under cooperative agreement by Associated Universities, Inc. C. Jin wishes to thank JIVE staff, in particular R.T. Schilizzi, L. Sjouwerman, H.J. van Langevelde and L.I. Gurvits for valuable discussions on various aspects of VLBI data analysis. S. Nair thanks Mark Walker for useful comments.

REFERENCES

Courbin, F., Lidman, C., Frye, B.L., et al. 1998, AJ, 499, L119-L123.

Frye, B.L., Courbin, F., Broadhurst, T.J., et al. 1999, ASP Conf. Proc. 156, ed. C.L. Carilli, S.J.E. Radford, K.M. Menten, & G.I. Langston, 240.

Garrett, M.A., Nair, S., Porcas, R.W., & Patnaik, A.R., 1997, *Visitas in Astronomy*, 41, 281.

Garrett, M.A., Porcas, R.W., Pedlar, A., et al. 1999, *NewAR*, 43, 519

Glenn Piner, B., Kingham, Kerry A., 1997, *ApJL*, 485, L61-63

Guirado, J.C., Jones, D.L., Lara, L., et al., 1999, *A&A*, 346, 393-396.

Jauncey, D.L., Reynolds, J.E., Tzioumis, A.K., et al., 1991, *Nature*, 352, 132.

Jin, C., Garrett, M.A., Nair, S., Porcas, R.W., Patnaik, A.R., 1999, *NewAR*, 43, 767

Jones, D.L., Preston, R.A., Murphy, D.W., et al., 1996, *ApJL*, 470, L23.

Kochanek, C.S. & Narayan, R., 1992, *ApJ*, 401, 461.

Kochanek, C.S., Kollat, T.S., & Bartelman, M., 1996, *ApJ*, 473, 610.

Lehár, J., Falco, E.E., Kochanek, C.S., et al. 2000, *ApJ*, 536, 584.

Leppänen, K.J., Zensus, J.A., & Diamond, P.J., 1995, *AJ*, 110, 2479

Lidman, C., Courbin, F., Meylan, G., Frye, B., & Welch, W.J.W., 1999, *ApJL*, 514, L57.

Lovell, J.E.J., Reynolds, J.E., Jauncey, D.L., et al., 1996, *ApJL*, 472, L5.

Lovell, J.E.J., Jauncey, D.L., Reynolds, J.E. et al. 1998, *ApJL*, 508:L51-L54.

Mattox, J.R., Schachter, J., Molnar, L., Hartman, R.C., & Patnaik, A.R., 1997, *ApJ*, 481, 95.

Nair, S., Narasimha, D., & Rao, A.P., 1993, *ApJ*, 407, 46.

Nair, S., Garrett, M.A., 2000, *BASI*, 28, 401.

Rao, A.P. & Subrahmanyam, R., 1988, *MNRAS*, 231, 229.

Rickett, B.J., 1990, *ARA&A*, 28, 561.

Romero, G.E., Benaglia, P., Combi, J.A., 1997, *A&AS*, 124, 307.

Shepherd, M.C., 1997, *Astronomical Data Analysis Software and Systems VI*, A.S.P. Conference Series, Vol. 125, 1997, Gareth Hunt and H. E. Payne, eds., p. 77.

Wambsganss, J., Paczynski, B., 1992, *ApJ*, 397, L1.

Wiklind, T., Combes, F., 1996, *Nature*, 379, 139.

Wiklind, T., Combes, F., 1999, *Proceedings of “Gravitational Lensing: Recent Progress and Future Goals”*, Boston University, 1999, Brainerd T.G. and Kochanek C.S. eds.